

# A symmoriiform chondrichthyan braincase and the origin of chimaeroid fishes

Michael I. Coates<sup>1</sup>, Robert W Gess<sup>2</sup>, John A. Finarelli<sup>3,4</sup>, Katharine E. Criswell<sup>1</sup> & Kristen Tietjen<sup>1</sup>

Chimaeroid fishes (Holocephali) are one of the four principal divisions of modern gnathostomes (jawed vertebrates). Despite only 47 described living species<sup>1</sup>, chimaeroids are the focus of resurgent interest as potential archives of genomic data<sup>2</sup> and for the unique perspective they provide on chondrichthyan and gnathostome ancestral conditions. Chimaeroids are also noteworthy for their highly derived body plan<sup>1,3,4</sup>. However, like other living groups with distinctive anatomies<sup>5</sup>, fossils have been of limited use in unravelling their evolutionary origin, as the earliest recognized examples already exhibit many of the specializations present in modern forms<sup>6,7</sup>. Here we report the results of a computed tomography analysis of *Dwykaselachus*, an enigmatic chondrichthyan braincase from the ~280 million year old Karoo sediments of South Africa<sup>8</sup>. Externally, the braincase is that of a symmoriid shark<sup>9–13</sup> and is by far the most complete uncrushed example yet discovered. Internally, the morphology exhibits otherwise characteristically chimaeroid specializations, including the otic labyrinth arrangement and the brain space configuration relative to exceptionally large orbits. These results have important implications for our view of modern chondrichthyan origins, add robust structure to the phylogeny of early crown group gnathostomes, reveal preconditions that suggest an initial morpho-functional basis for the derived chimaeroid cranium, and shed new light on the chondrichthyan response to the extinction at the end of the Devonian period.

The nodule-enclosed braincase of *Dwykaselachus oosthuizeni* Oelofsen<sup>8</sup> South African Museum (SAM) K5840 (Fig. 1 and Extended Data Fig. 1a–c) derives from the base of the Prince Albert Formation (Ecca Group, Karoo Supergroup)<sup>8</sup>. Early Permian dating estimates vary from the early Artinskian<sup>14</sup> to the latest Kungurian stage<sup>15</sup>. The braincase is intact from anterior to posterior extremities and mostly uncrushed, despite consisting of no more than thin monolayered tessellate calcified cartilage (Extended Data Fig. 1d). Computed tomography (CT) analysis reveals a symmoriiform external morphology (Fig. 1 and Supplementary Video 1) resembling a three-dimensionally preserved, although anteriorly incomplete, braincase attributed to *Cobelodus*<sup>9</sup> (Extended Data Fig. 2a, b). Consequently, important new information especially concerns the anterior orbit and pre-orbital regions (Extended Data Fig. 3) and the cranial endocast (Fig. 2a, b and Extended Data Fig. 4). See Supplementary Information for detailed description.

The unusually complete ethmoid cartilages (Fig. 1 and Extended Data Fig. 3) include large hemispherical nasal capsules situated above wide subnasal spaces. As in chimaeroids and certain elasmobranchs<sup>16,17</sup>, the capsules join at an internasal plate (Extended Data Figs 3 and 5a), the anterior flare of which was previously identified as a precerebral fontanelle<sup>8</sup>. Like iniopterygians<sup>18</sup>, the nasal capsules are bridged by an internasal groove (Fig. 1b). Each capsule roof is shorter than the floor, suggesting that, unlike many sharks<sup>17</sup>, the narial openings were directed

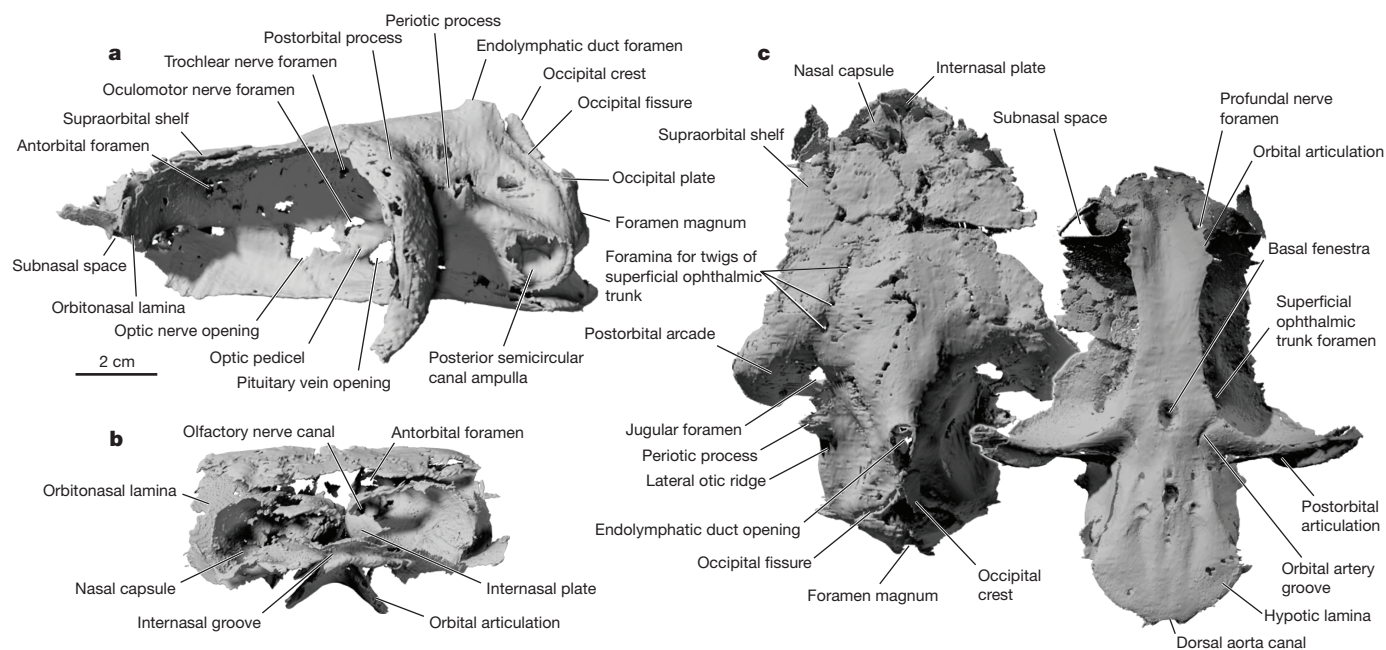


**Figure 1** | The braincase of *D. oosthuizeni* Oelofsen 1986 modelled from high-resolution CT of SAM K5840. **a–c**, In left lateral view (**a**), in anterior view (**b**) and in dorsal (left) and ventral views (right; **c**).

<sup>1</sup>Department of Organismal Biology and Anatomy, University of Chicago, Chicago, Illinois 60637-1508, USA. <sup>2</sup>Geology Department and Albany Museum, Rhodes University, Grahamstown 6139, South Africa. <sup>3</sup>UCD School of Biology and Environmental Science, UCD Science Education and Research Centre, University College Dublin, Belfield, Dublin 4, Ireland. <sup>4</sup>UCD Earth Institute, University College Dublin, Belfield, Dublin 4, Ireland.

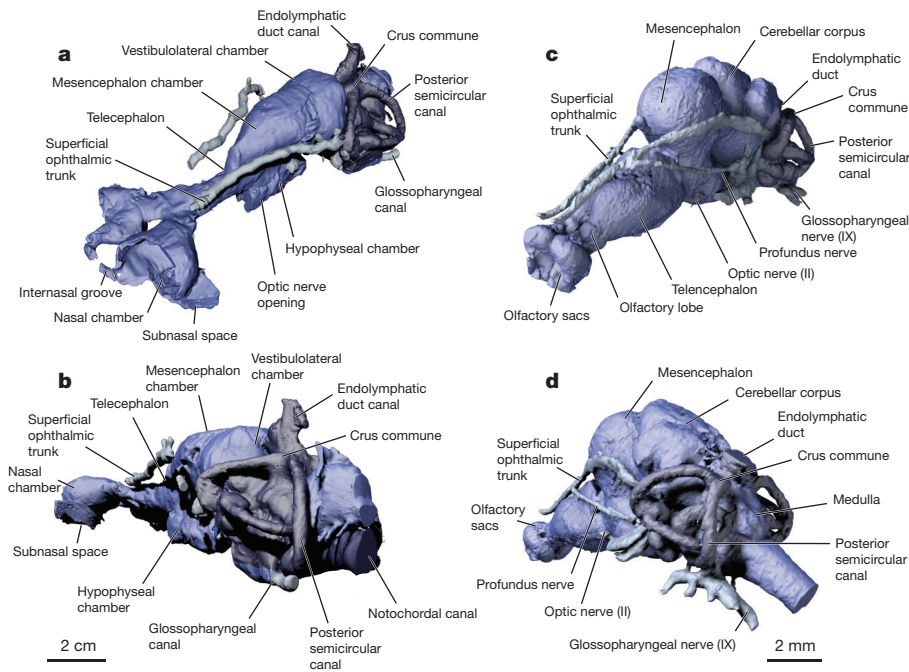


**Figure 2 | *Dwykasselachus* and *Callorhynchus milii* endocranial anatomy. a, b, *Dwykasselachus* virtual endocast based on high-resolution CT of SAM K5840. c, d, *Callorhynchus* hatchling virtual morphology of brain, otic labyrinth and major cranial nerves based on high-resolution CT. a–d, In dorsal and anterolateral aspect (a, c) and in posterolateral view (b, d).**

slightly dorsally. The capsule wall openings include a canal for the olfactory nerve (nerve I), a foramen for the profundus nerve (nerve V), and an opening in the floor (Extended Data Fig. 3c), resembling the subnasal fenestra of *Doliodus*<sup>19</sup>, which communicates with the subnasal space (Extended Data Fig. 3d, e).

A precerebral fontanelle, a signature of non-chimaeroid chondrichthyans, is either absent or reduced. The braincase roof is nearly complete (Fig. 1c); if present, the fontanelle was probably restricted to a space above the rear of the nasal capsules. Each supraorbital shelf bears a groove traversing the ventral surface, marking the path of the superficial ophthalmic trunk (nerve VII) towards an antorbital foramen (Fig. 2a, b and Extended Data Figs 3, 5a), the position of which matches the orbital entrance of the chimaeroid ethmoid canal<sup>13,16</sup> (compare morphologies in Supplementary Videos 1 and 2). Although these nerves entered the rostral portion of the cranial cavity, there is no trace of an enclosed ethmoid canal. Posteriorly, each supraorbital shelf extends as a wide and deep postorbital process and arcade like those of *Cobelodus*<sup>9</sup> and *Akmonistion*<sup>10</sup>, surrounding a large subcircular jugular foramen (Extended Data Fig. 6a, b).

*Dwykasselachus* has exceptionally large orbits (Fig. 1a, c and Extended Data Fig. 5a) like other symmorids (Extended Data Fig. 2) and holocephalans (Fig. 3). An interorbital septum is present<sup>3,9</sup>, but is restricted to an area anterior to the optic nerve (nerve II) foramen (Extended Data Fig. 7) and posterior to a broad opening connecting left and right orbits directly behind the orbitonasal lamina. Below this interorbital foramen (Extended Data Fig. 5a), the narrow suborbital shelf broadens to form a grooved orbital articulation with the palate.

The cruciform basicranial outline includes wide, slender postorbital arcades (Fig. 1c) resembling *Akmonistion*<sup>10</sup> (Extended Data Fig. 2h). Anteriorly, the base of the internasal plate is deeply concave between the subnasal spaces (Extended Data Fig. 5a) that are here recognizable as openings identified as nasal capsules in previous interpretations of symmoriform neurocrania<sup>12</sup>. Posteriorly, the cranial floor exhibits the characteristic narrow waist of symmorids<sup>9,10</sup>, with the aortic network contained mostly within the basicranial cartilage anterior to a single opening for the dorsal aorta at the base of the occiput.

The dorsal ridge of the otic roof encloses a chimaeroid-like endolymphatic foramen<sup>16</sup> (Fig. 1a, c and Extended Data Fig. 5b), and the

lateral otic ridge bears a large periotic process similar to *Cobelodus*<sup>9</sup>. A paired crest extends dorsally from the compact occipital arch (Extended Data Figs 6c, d and 8a, b) towards the dorsal ridge apex. Rather than wedging between the otic capsules, the usual condition in Recent and fossil sharks<sup>17</sup>, the occipital plate fits around the rear of the otic region, much like osteichthyans (Extended Data

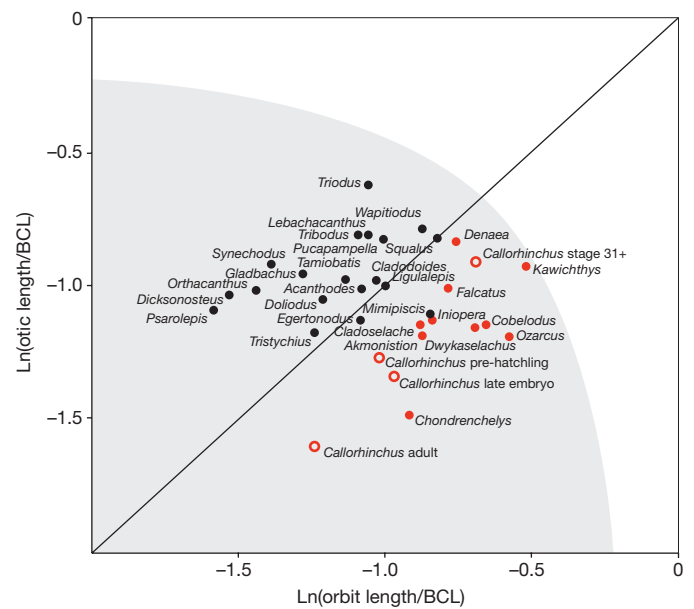


**Figure 3 | Plot of orbit versus log-otic capsule length, normalized to basicranial length. Holocephalans, red; non-holocephalans, black. Line indicates identically sized orbital and otic regions; relative size increases from bottom left to top right. White region comprises impossible geometries (orbit plus otic exceeds cranium length). With the exception of *Mimipiscis*, holocephalans occupy a distinct region with relatively larger orbits. Open red circles mark *C. milii* growth series; age increases from top to bottom. Orbital and otic regions grow with negative allometry with respect to overall skull length, however, orbit size relative to the otic capsule increases through ontogeny. BCL, basicranial length.**

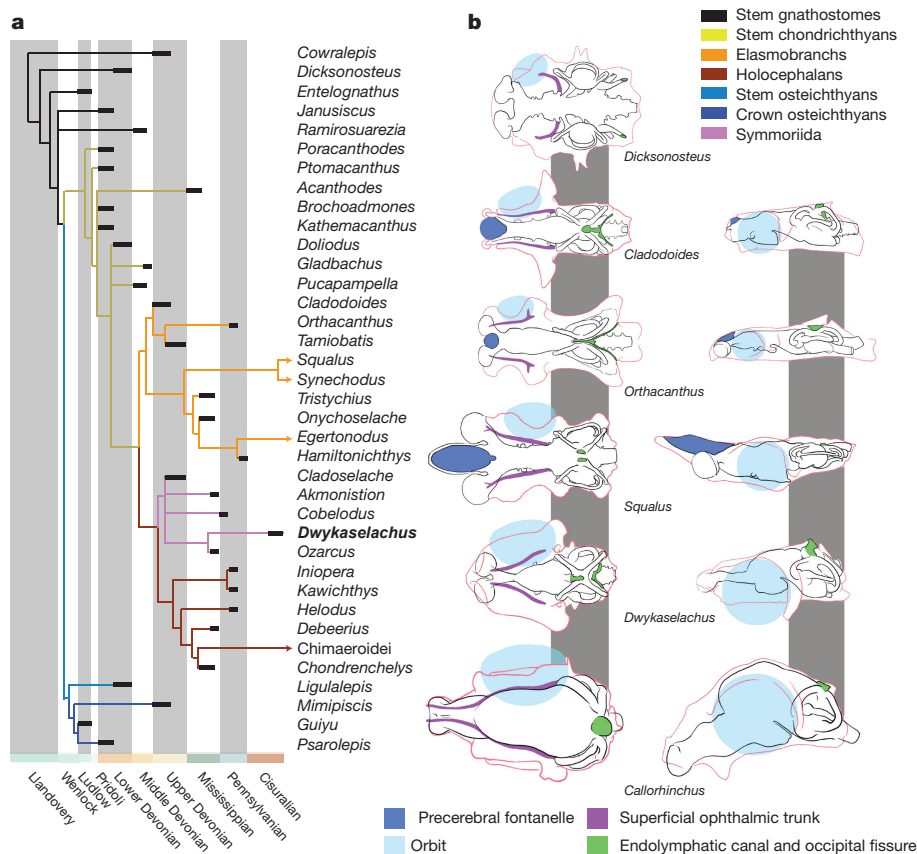


**Figure 4 | Phylogeny of early chondrichthyans scaled to stratigraphy, with comparative morphology of selected chondrichthyan and outgroup crania.** **a**, Strict consensus cladogram of the phylogenetic analyses plotted against the geological timescale. **b**, Cranial outlines (red) and endocranial space outlines (black) in dorsal and lateral views,

Fig. 8c, d). Ventrally, however, the parachordal cartilage broadens as a characteristic chondrichthyan hypotic lamina<sup>9,20</sup>.

Unexpectedly, the endocast of *Dwykasselachus* in dorsal view (Fig. 2a, b, Extended Data Fig. 4 and Supplementary Video 1) resembles conditions observed in both actinopterygians<sup>21</sup> and chimaeroids (Fig. 2c, d and Supplementary Video 2), wherein the bulk of the brain is located posterior to large orbits. The vestibulolateral chamber, located between the anterior semicircular canals, projects above the level of the otic labyrinth (Fig. 2b, d and Extended Data Fig. 7), and anteriorly, the mesencephalon chamber narrows into a slender space for the telencephalon. Within this interorbital space, boundaries between the olfactory lobe and tract territories are indistinct before diverging anteriorly into the nasal capsules (Fig. 2a and Extended Data Figs 3g, 4a).

In lateral view, more characteristically chondrichthyan features are visible, including the large hypophyseal chamber and dorsally projecting endolymphatic duct<sup>1,9,17</sup> (Fig. 2a, b and Extended Data Figs 4b, 7). As in chimaeroids, the duct space lies slightly anterior to the crus commune, exiting the neurocranial roof through a midline opening (Extended Data Fig. 5b). The most visible shared specialization with chimaeroids, in contrast to actinopterygians<sup>21</sup>, is the offset between the dorsally prominent mesencephalon chamber and the ventral level of the telencephalon space<sup>20,22</sup> (Fig. 2b, d). Thus, *Dwykasselachus*, and probably *Cobelodus*, share the characteristic chimaeroid elevation of the midbrain, relative to forebrain and hindbrain (Extended Data Fig. 9), above a well-developed dorsum sellae (Extended Data Fig. 7).

Phylogenetic analyses establish the importance of the shared similarities between *Dwykasselachus* and chimaeroids, recovering symmoriiforms as sister clade to inioptrygians and holocephalans

aligned and sized to match dimensions of the otic capsules (standardized to grey column width); relative orbit sizes, paths of superficial ophthalmic trunks, endolymphatic openings and precerebral fontanelles are colour coded for direct comparison. Data sources for each genus are provided in Supplementary Information.

(Fig. 4a and Extended Data Fig. 10). Similar hypotheses have been offered previously<sup>23–25</sup>, but lacked the detailed fossil chondrichthyan data used here, and the stable branching pattern of the resultant tree. Expansion of holocephalan stem membership moves the chondrichthyan crown group divergence<sup>7</sup> to a deeper phylogenetic node (Fig. 4a), implying a minimum age for the elasmobranch–chimaeroid split within the uppermost Devonian, consistent with isolated but phylogenetically uncertain dental remains attributed to holocephalans<sup>4</sup>. A further implication is that the post-Devonian chondrichthyan evolutionary radiation<sup>26</sup> was populated by stem holocephalans to a far greater extent than has previously been appreciated.

A monophyletic Symmoriida including *Cladoseelache* as stem holocephalans challenges continued use of these taxa as models for primitive chondrichthyan and gnathostome conditions<sup>11,13,24</sup>, separating synapomorphies specific to the Symmoriida from those shared with the origin of inioptrygians and the lineage leading to chimaeroids, thus defining the symmoriiform morphotype (*sensu lato*)<sup>9,27</sup> (Supplementary Table 3). Initial cranial specializations of the holocephalan total group include a chimaera-like endolymphatic duct opening, ventral displacement of the forebrain endocranial cavity roof, and extremely large orbits (Extended Data Fig. 9a). Indeed, orbit enlargement appears to be entrenched before the large-scale modifications of the ethmoid region, jaws and dentition (Figs 3 and 4b), including changes that probably influenced subsequent patterns of cranial morphological disparity<sup>3,4,16</sup>. Large orbit size is also an important indicator of visual system evolution with implications for niche specialization<sup>28</sup>. As highly visual foragers, large eye diameter in fishes is a signal of dim-light vision<sup>29</sup>, and the prominent orbits of early and Recent chimaeroids<sup>30</sup> (Fig. 3) suggest a corresponding functional adaptation. Here, the large orbits of symmoriiforms suggest that

adaptation to light-limited conditions originated earlier in phylogeny, probably predisposing the earliest members of the holocephalan clade for subsequent exploitation of deep-marine habitats<sup>1,30</sup>.

**Online Content** Methods, along with any additional Extended Data display items and Source Data, are available in the online version of the paper; references unique to these sections appear only in the online paper.

**Received 9 June; accepted 18 November 2016.**

**Published online 4 January 2017.**

- Didier, D. A., Kemper, J. M. & Ebert, D. A. in *Biology of Sharks and Their Relatives* (eds Carrier, J. C., Musick, J. A. & Heithaus, M. R.) 97–122 (CRC, 2012).
- Venkatesh, B. *et al.* Elephant shark genome provides unique insights into gnathostome evolution. *Nature* **505**, 174–179 (2014).
- Patterson, C. The phylogeny of the chimaeroids. *Phil. Trans. R. Soc. Lond. B* **249**, 101–219 (1965).
- Stahl, B. J. in *Handbook of Paleoichthyology* Vol. 4 (ed. Schultze, H.-P.) (Friedrich Pfeil, 1999).
- Simmons, N. B., Seymour, K. L., Habersetzer, J. & Gunnell, G. F. Primitive Early Eocene bat from Wyoming and the evolution of flight and echolocation. *Nature* **451**, 818–821 (2008).
- Grogan, E. D., Lund, R. & Greenfest-Allen, E. in *Biology of Sharks and Their Relatives* (eds Carrier, J. C., Musick, J. A. & Heithaus, M. R.) 3–29 (CRC, 2012).
- Finarelli, J. A. & Coates, M. I. *Chondrenchelys problematica* (Traquair, 1888) redescribed: a Lower Carboniferous, eel-like holocephalan from Scotland. *Earth Env. Sci. Trans. R. Soc. Edinb.* **105**, 1–25 (2014).
- Oelofsen, B. W. in *Indo-Pacific Fish Biology: Proceedings of the Second International Conference on Indo-Pacific Fishes* (eds Uyeno, T., Arai, R., Taniuchi, T. & Matsuura, K.) 107–124 (Ichthyological Society of Japan, 1986).
- Maisey, J. G. The braincase in Paleozoic symmoriform and cladoselelchian sharks. *Bull. Am. Mus. Nat. Hist.* **307**, 1–122 (2007).
- Coates, M. I. & Sequeira, S. E. K. The braincase of a primitive shark. *Trans. R. Soc. Edinb. Earth Sci.* **89**, 63–85 (1998).
- Zangerl, R. & Case, G. R. *Cobelodus aculeatus* (Cope), an anacanthid shark from the Pennsylvanian black shales of North America. *Palaeontographica A* **154**, 107–157 (1976).
- Williams, M. E. The “cladodont level” sharks of the Pennsylvanian black shales of central North America. *Palaeontographica A* **190**, 83–158 (1985).
- Pradel, A., Maisey, J. G., Tafforeau, P., Mapes, R. H. & Mallatt, J. A. Palaeozoic shark with osteichthyan-like branchial arches. *Nature* **509**, 608–611 (2014).
- Bangert, B., Stollhofen, H., Lorenz, V. & Armstrong, R. The geochronology and significance of ash-fall tuffs in the glaciogenic Carboniferous–Permian Dwyka Group of Namibia and South Africa. *J. Afr. Earth Sci.* **29**, 33–49 (1999).
- McKay, M. P. *et al.* U-PB zircon tuff geochronology from the Karoo Basin, South Africa: implications of zircon recycling on stratigraphic age controls. *Int. Geol. Rev.* **57**, 393–410 (2015).
- De Beer, G. R. & Moy-Thomas, J. A. On the skull of Holocephali. *Phil. Trans. R. Soc. Lond. B* **224**, 287–312 (1935).
- Schaeffer, B. The xenacanth shark neurocranium, with comments on elasmobranch monophyly. *Bull. Am. Mus. Nat. Hist.* **169**, 1–66 (1981).
- Pradel, A. Skull and brain anatomy of Late Carboniferous Sibirhynchidae (Chondrichthyes, Iniopterygia) from Kansas and Oklahoma (USA). *Geodiversitas* **32**, 595–661 (2010).
- Maisey, J. G., Miller, R. & Turner, S. The braincase of the chondrichthyan *Doliodus* from the Lower Devonian Campbellton Formation of New Brunswick, Canada. *Acta Zoologica* **90** (Suppl. 1), 109–122 (2009).
- Pradel, A., Didier, D., Casane, D., Tafforeau, P. & Maisey, J. G. Holocephalan embryo provides new information on the evolution of the glossopharyngeal nerve, metotic fissure and parachordal plate in gnathostomes. *PLoS One* **8**, e66988 (2013).
- Giles, S. & Friedman, M. Virtual reconstruction of endocast anatomy in early ray-finned fishes (Osteichthyes, Actinopterygii). *J. Paleontol.* **88**, 636–651 (2014).
- Howard, L. E. *et al.* Functional nasal morphology of chimaerid fishes. *J. Morphol.* **274**, 987–1009 (2013).
- Coates, M. I. & Sequeira, S. E. K. in *Major Events in Early Vertebrate Evolution* (ed. Ahlberg, P. E.) 241–262 (Taylor & Francis, 2001).
- Janvier, P. *Early Vertebrates* (Clarendon, 1996).
- Giles, S., Friedman, M. & Brazeau, M. D. Osteichthyan-like cranial conditions in an Early Devonian stem gnathostome. *Nature* **520**, 82–85 (2015).
- Friedman, M. & Sallan, L. C. Five hundred million years of extinction and recovery: a Phanerozoic survey of large-scale diversity patterns in fishes. *Palaeontology* **55**, 707–742 (2012).
- Schmitz, L., Tafforeau, P., Maisey, J. G. & Janvier, P. A new paleozoic Symmoriformes (Chondrichthyes) from the late Carboniferous of Kansas (USA) and cladistic analysis of early chondrichthyans. *PLoS One* **6**, e24938 (2011).
- Cronin, T. W., Johnsen, S., Marshall, N. J. & Warrant, E. J. *Visual Ecology* (Princeton Univ. Press, 2014).
- Schmitz, L. & Wainwright, P. C. Nocturnality constrains morphological and functional diversity in the eyes of reef fishes. *BMC Evol. Biol.* **11**, 338 (2011).
- Lisney, T. J. A review of the sensory biology of chimaeroid fishes (Chondrichthyes; Holocephali). *Rev. Fish Biol. Fish.* **20**, 571–990 (2010).

**Supplementary Information** is available in the online version of the paper.

**Acknowledgements** We thank the Evolutionary Studies Institute micro-CT scanning unit at the University of the Witwatersrand in Johannesburg, South Africa, for provision of scanning facilities and K. Carlson and K. Jakata for technical assistance. We thank R. Smith and the staff of the South African Museum, Cape Town, for access and loan of specimen. We thank A. Gillis for the donation of *Callorhynchus milii* embryos and hatchlings. This work was supported by grants DEB-0917922 and DEB-1541491 from the National Science Foundation (to M.I.C.), and a research grant from the National Research Foundation/Department of Science and Technology South African Centre of Excellence in Palaeosciences (to R.W.G.).

**Author Contributions** This project was conceived by M.I.C. and R.W.G. and developed by M.I.C., R.W.G., J.A.F. and K.E.C. CT scanning of *Moythomasia durgaringa* was conducted by K.T.; renderings and animations of CT scans and graphics were completed by K.T. with input from M.I.C., K.E.C. and J.A.F. *C. milii* preparation and staining were completed by K.E.C. Phylogenetic data were collected by M.I.C., K.E.C. and J.A.F. Phylogenetic analyses were completed by J.A.F. and M.I.C. Morphometric data were collected by M.I.C. and K.E.C.; analysis was completed by M.I.C., K.E.C. and J.A.F. Manuscript and supplementary text preparation was undertaken by M.I.C., R.W.G. and J.A.F. with input from K.E.C.

**Author Information** Reprints and permissions information is available at [www.nature.com/reprints](http://www.nature.com/reprints). The authors declare no competing financial interests. Readers are welcome to comment on the online version of the paper. Correspondence and requests for materials should be addressed to M.I.C. ([mcoates@uchicago.edu](mailto:mcoates@uchicago.edu)).

**Reviewer Information** *Nature* thanks M. Friedman, P. Janvier and the other anonymous reviewer(s) for their contribution to the peer review of this work.

## METHODS

**X-ray CT.** The scan of *Dwykaselachus* was performed using a NIKON XTH 225/320 LC dual source industrial microCT system housed at the Evolutionary Studies Institute, University of the Witwatersrand, Johannesburg, South Africa. Scan parameters: 185 kV, 0.185 mA, 2 s acquisition time, 3.6 mm copper used to filter out the low energy X-ray photons, voxel size 0.072 mm. Total slices: 1,610 dorsal section of nodule (sample A), 1,750 ventral section of nodule (sample B); 16-bit TIFF images collected; 8-bit jpg version used for reconstruction. The scan of *C. milii* was completed by J. Maisano at the University of Texas at Austin, High-resolution X-ray CT Facility. Scan parameters: 70 kV, 10 W, 1.5 s acquisition time, no filter used, voxel size 0.0216 mm. Total slices: 965; 16-bit TIFF images collected; 8-bit jpg version used for reconstruction. The scan of *Moythomasia durgaringa* was completed by K.T. at the University of Chicago, Department of Organismal Biology and Anatomy PaleoCT Scan facility. Scan parameters: 160 kV, 0.28 mA, 1 s acquisition time, no filter used, voxel size 0.0399 mm. Total slices: 2,093; 16-bit TIFF images collected; 8-bit jpg version used for reconstruction.

**Anatomical reconstruction.** Mimics v. 17 (<http://www.biomedical.materialise.com/mimics>; Materialise, Leuven, Belgium) was used for the three-dimensional modelling, including segmentation, three-dimensional object rendering, STL polygon creation and kinematics. 3D Studio Max (<http://www.autodesk.com/products/3ds-max>; Autodesk, San Rafael, USA) was used for further editing of the STLs (colour, texture, lighting), kinematics, and mirroring for the final restoration. Restorations of *Dwykaselachus* combine data samples A and B.

**Phylogenetic analyses.** The character matrix consists of 37 taxa, 35 ingroup taxa and two outgroups (*Cowralepis* and *Dicksonosteus*) coded for 145 morphological characters. Selected taxa provide broad coverage of early chondrichthyan groups, including genera that are widely agreed to branch from elasmobranch and holocephalan stems and those that are known from substantial body-fossil remains. *Squalus acanthias* provides an exemplar for Recent elasmobranch conditions, and a combination of character scores from *C. milii* and *Hydrolagus colliciei* exemplify Recent chimaeroid conditions. Character-rich neurocrania are known in 15/23 euchondrichthyans in the data set; 10/23 include CT-generated cranial data. Non-euchondrichthyan taxa are represented by five ‘acanthodian’ genera, and a further nine genera cover non-chondrichthyan Palaeozoic gnathostomes. Full details, additional references and justification of character choices are provided in the Supplementary Information. Character coding average across the matrix is 58.2% complete for the ingroup taxa, with wide variance in completeness among ingroup taxa (29.0%, *Poracanthodes* to 92.4%, *Egertonodus*).

We performed a heuristic search in PAUP\*4.147 (ref. 31), using 10,000 random sequence additions. We assessed nodal support through bootstrapping<sup>32</sup> and Bremer decay indices<sup>33</sup>. For the bootstrap, we performed 1,000 bootstrap replicates, employing a heuristic search for each replicate with 50 random sequence additions, limited to 5 million rearrangements per addition.

bootstrap nrep = 1000 search = heuristic/addseq = random nrep  
= 50 limitperrep = yes rearrlimit = 5000000;

Bremer decay indices were calculated for the nodes present in the strict consensus of the most parsimonious cladograms for the full data set using the Perl script AutoDecay<sup>34</sup>, in conjunction with PAUP\* (ref. 31), using 1,000 random sequence additions for each node. Character state transitions by node for the strict consensus cladogram of the MPTs were reconstructed in PAUP\* (ref. 31) assuming hard polytomies and employing DELTRAN optimization. Further taxon and character exclusion analyses were performed using the heuristic searches in PAUP\*4.147 (ref. 31) to assess the robustness of the topology recovered in the all-taxa analysis. For the taxon exclusion analyses, chondrichthyan taxa were removed from the analysis one by one, and the impact on the nodes recovered in the strict consensus of the MPTs was noted for each excluded taxon. Character partitions considered neurocranial (characters 62–122), and non-neurocranial partitions, as well as the set of characters that were either newly added to the data matrix or were dramatically recoded as a result of the new CT data provided by *Dwykaselachus* (characters 65, 67, 73, 80, 85, 97, 101, 107, 115, 120).

In addition, we performed a Bayesian phylogenetic analysis<sup>35,36</sup> of the morphological data matrix<sup>37</sup> in Mr. Bayes 3.2.5 (refs 38, 39). We implemented an MCMCMC search using the ‘variable characters only’ coding option for the cladistic character data in our matrix. Prior probabilities for character stationary frequencies were estimated using the symmetric Dirichlet prior, allowing for rate heterogeneity among characters by specifying gamma-distributed rates.

Lset rates = gamma coding = variable nbetacat = 5;

Prset applyto = (all) symdirihyperpr = fixed(2.0) ratepr = variable;

The search was run for five million generations, employing two runs of four chains. Trees were sampled for each run every 1,000 generations, and a majority rule consensus of the sampled trees was computed from this output, using a 25% relative burnin. No statistical methods were used to predetermine sample size. The experiments were not randomized. The investigators were not blinded to allocation during experiments and outcome assessment.

**Phylogenetic results.** The cladistic analysis yielded 240 trees of 275 steps (consistency index = 0.542, retention index = 0.766). Figure 4 shows the strict consensus of results scaled to the geological timescale of Gradstein *et al.*<sup>40</sup> and Extended Data Fig. 10a shows the strict consensus tree with nodal support values as assessed through bootstrapping and Bremer decay indices. Unambiguous character state transitions are listed in Supplementary Table 3. Extended Data Fig. 10b shows the majority rule consensus tree of Bayesian analysis. Both consensus trees are well resolved with highly congruent branching patterns. In both trees, symmoriiforms and iniopterygians are recovered as stem holocephalans, with ctenacanth, xenacanth and hybodontiforms as stem elasmobranchs. Both Bayesian and MP trees also include *Doliodus*, *Pucapampella*, *Gladbachus* and a suite of ‘acanthodians’ as stem chondrichthyans, consistent with results of recent, more inclusive analyses of early gnathostome phylogeny<sup>25,41</sup>. Node support values are highest for the Chondrichthyes total group (‘Euchondrichthyes’ of Grogan *et al.*<sup>6</sup>) (node 5), *Synechodus* and *Squalus* (node 12), and the holocephalan total group (‘Paraselachii’ of Grogan *et al.*<sup>6</sup>) (node 18).

The topology of the strict consensus of the MPTs is preserved even if we exclude *Dwykaselachus* from cladistic analysis. This is probably due to the widespread influence that the new CT data on characters and scoring throughout chondrichthyans in the data set. Tests of individual fossil ‘euchondrichthyan’ (*sensu* Pradel *et al.*<sup>13</sup>) exclusions demonstrate that the topology of the chondrichthyan phylogeny observed in the all-taxa analysis is exceedingly stable. Supplementary Table 4 shows that none of these taxa exerts a dominant influence on the resultant branching patterns, with all of the major clade interrelationships preserved. Strict consensus trees from exclusion sets for taxa with: (1) greater individual influence on tree topology (*Chondrenchelys*, *Egertonodus*, *Iniopera*, *Ozarcus*, *Synechodus*, *Tristychius* and *Tamiobatis*), and (2) lesser influence (*Akmonistion*, *Cladodoidea*, *Cladoselache*, *Cobelodus*, *Debeeri*, *Doliodus*, *Dwykaselachus*, *Hamiltonichthys*, *Helodus*, *Orthacanthus*, *Pucapampella*), as well as, (3) *Gladbachus* (deletion of which results in a resolved upper stem group) present the same fundamental clade relationships, with trees that are generally congruent with the all-taxa strict consensus in Extended Data Fig. 10a.

Character partition tests reveal a structured division within the data set, showing that the phylogenetic signal responsible for the recovery of symmoriiforms with holocephalans resides primarily in the neurocranial data. Analysis excluding neurocranial characters delivers an unresolved Chondrichthyes total group (84 characters retained; taxa consisting of an isolated neurocranium excluded; 6,696 trees of 141 steps) with informative tree structure mostly lost. When only neurocranial characters are retained the result is a well-resolved consensus tree in which a holocephalans and symmoriiform clade is sister to elasmobranchs (61 characters retained; taxa lacking preserved neurocrania excluded; 54 trees of 113 steps). Some indication of the *Dwykaselachus* influence on data set composition and phylogenetic signal is provided by deletion of the set of characters that were either novel characters or recoded in response to the new CT-generated data. It is noteworthy that characters that have previously been hypothesized as synapomorphies of symmoriiforms and holocephalans<sup>23,25</sup> were retained in this character partition analysis. A strict consensus cladogram of 360 trees (256 steps) recovered four monophyletic clades (a ctenacanth/xenacanth clade, an elasmobranch clade, a symmoriiform clade, and a holocephalan clade) at the chondrichthyan stem lineage apex, but was unresolved among them (Extended Data Fig. 10a: nodes 16, 11, 24 and 19 preserved, but nodes 10 and 18 lost).

Janvier<sup>24</sup> first posited a close relationship between holocephalans and symmoriiforms (“peculiar fossil forms that are otherwise quite unlike chimaeras”). This hypothesis was first formally tested by Coates and Sequeira<sup>23</sup>, and was recently recovered as part of a broader analysis by Giles *et al.*<sup>25</sup> of early crown gnathostomes. This holocephalan–symmoriiform hypothesis originally provided an alternative to the widely accepted proposal that symmoriiforms were stem elasmobranchs<sup>7,11,17,42–44</sup>. More recently, both hypotheses have been displaced by analyses that recover symmoriiforms as stem chondrichthyans<sup>27,45–49</sup>, in agreement with Maisey’s<sup>50</sup> foundational examination of chondrichthyan characters and phylogeny.

Definitions of what constitutes a ‘symmoriiform’ have varied from early, restrictive memberships<sup>12,24,51</sup> defined mostly by postcranial features<sup>23</sup>, to more recent discussions of symmoriiforms among ‘cladodont’ sharks<sup>9,13,27,45</sup>, which characterize the group using cranial synapomorphies. ‘Symmoriiform cranial conditions’, as a concept of morphotype not clade membership, have come to

mean big orbits, broad roofs, narrow bases, large arcades, narrow waists, short otic regions, and compact occiputs. Indeed, these qualifications underlie the Pradel *et al.*<sup>27</sup> characterization of *Kawichthys* as a symmoriiform, and the informal recognition of *Dwykasselachus* as a likely member of this group<sup>9</sup>.

The present hypothesis identifies a symmoriiform clade, which includes stethacanthids and cladoselachians, alongside an exemplary traditional member of this group, *Cobelodus*<sup>11,51</sup>. This clade is defined by a mixture of synapomorphies from neurocranial, viscerocranial and postcranial skeletal regions (Supplementary Table 3, nodes 18 to 24), however, important signatures of the symmoriiform, *sensu lato*, cranial morphotype (a large orbit, trigeminofacial recess absence, subcircular endolymphatic foramen presence, and morphological indication of a dorsal aortic split anterior to the occiput) are now among the synapomorphies that define the holocephalan total group (Supplementary Table 3, nodes 9 to 18). It is in this sense that symmoriids, *sensu stricto*, iniopterygians, as well as more crownward holocephalans all emerge from a general, symmoriiform suite of initial morphological conditions.

Symmoriiform assignment to the holocephalan stem lineage expands the range of morphological conditions characterizing early clade members, and increases the total group membership beyond Zangerl's<sup>52</sup> Subterbranchialia (see also Stahl<sup>4</sup>). Notably, under the present hypothesis, 12 out of 19 divisions named in Janvier's (table 4.6 in ref. 24) classification of Chondrichthyes are total group holocephalans. Previous hypotheses that eugeneodontids<sup>51</sup> also branch from the holocephalan stem<sup>6,53</sup> are supported by the presence of a heterocercal high aspect ratio tail with specialized caudal neural arch cartilages (otherwise characteristic of symmoriiforms), in addition to enlarged orbits relative to otic dimensions. Other groups widely accepted as early holocephalans that were not included in the present analysis include petalodonts, cochliodonts, psammodonts, copodonts and menaspiforms.

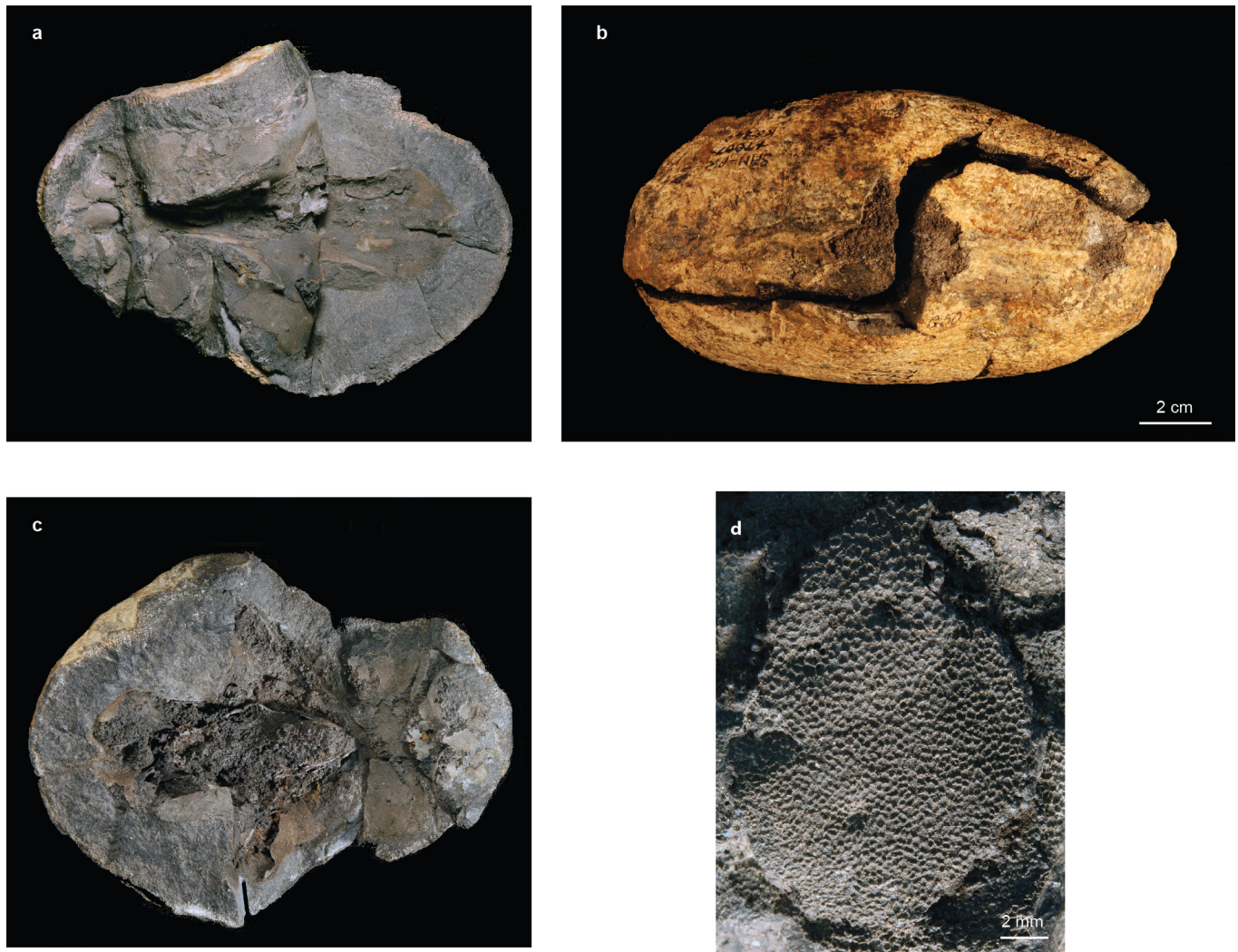
The node minimum age for crown Chondrichthyes is currently set within the mid-Viséan stage, at 334 million years ago (Ma) (ref. 54). However, present results suggest that it should be moved to at least the uppermost Fammenian stage, at 358 Ma, based on the results of the current cladistic analyses, and fossil evidence in the form of at least two Fammenian stage symmoriiform genera known from substantial skeletal remains<sup>12,45</sup>, three Fammenian likely stem holocephalan toothplate genera<sup>4</sup>, two likely stem holocephalan toothplate genera in the Frasnian stage (372–382 Ma)<sup>4</sup>, and a putative holocephalan toothplate fragment in the Givetian stage<sup>55</sup> (382–387 Ma).

**Morphometric analysis.** Data for orbital lengths, otic capsule lengths and basicranial lengths (Supplementary Table 1) were obtained from the crania for 33 genera, including 14 taxa in the holocephalan total group ('holocephalans'), here taken to include symmoriiforms following the results of the phylogenetic analysis, and 19 non-holocephalans. Where possible, taxa were used from the set of those included in the phylogenetic analysis; several additional taxa were also included. Mann-Whitney tests demonstrate that both  $\ln(\text{orbit length}/\text{BCL})$  and  $\ln(\text{otic length}/\text{BCL})$  differ significantly between the holocephalan and non-holocephalan samples ( $P < 0.0001$  and  $0.0028$ , respectively) (see Fig. 3). Holocephalan taxa have larger relative orbit lengths than non-holocephalan taxa, whereas non-holocephalans have relatively larger otic capsules (Supplementary Table 2).

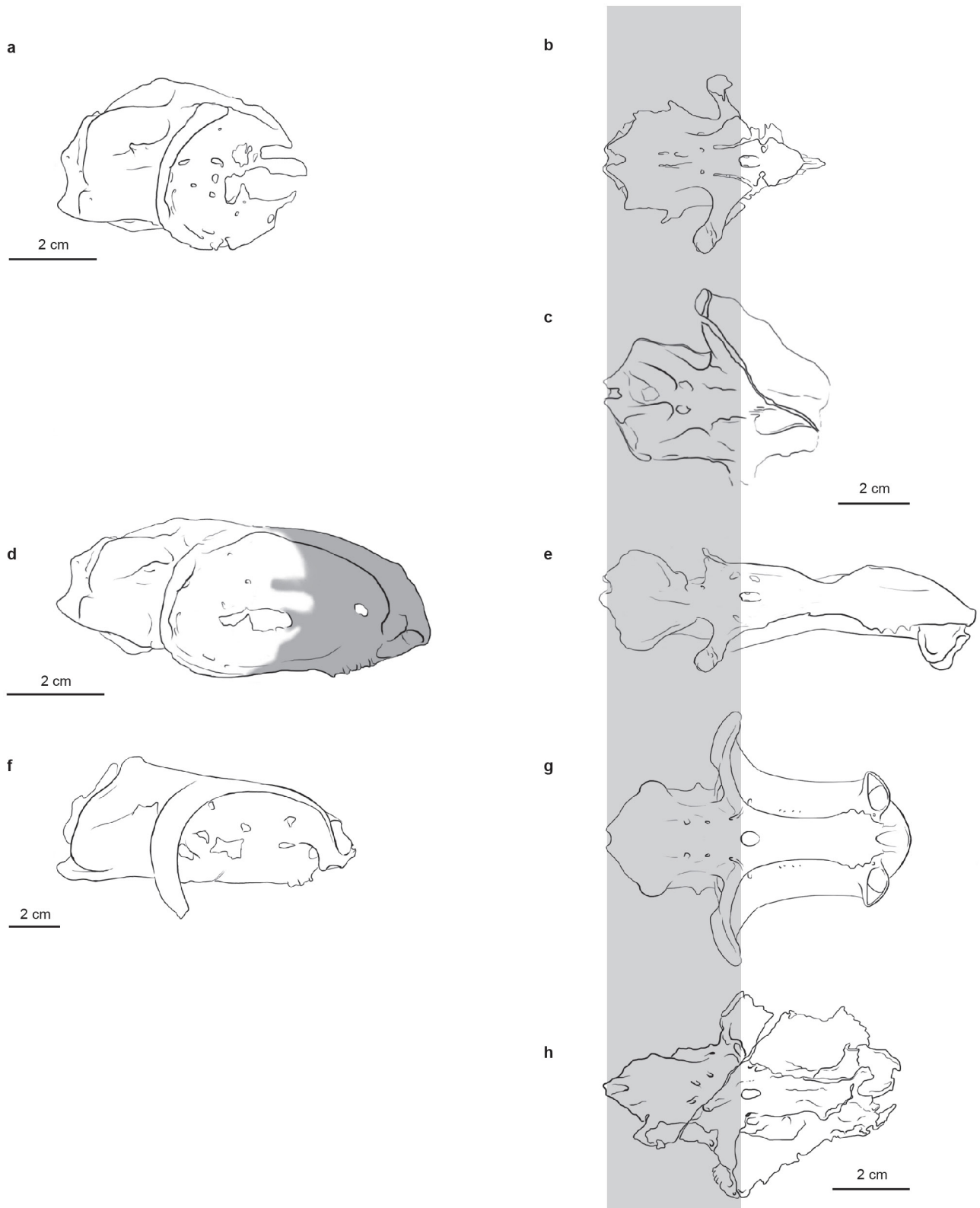
The ontogenetic series for the modern chimaeroid *C. milii* (open red circles in Fig. 3) demonstrate a negative ontogenetic allometry for both the orbital and otic portions of the skull with respect to overall skull length. In addition, orbit size relative to otic capsule length increases through development, with orbit size going from ~125% of otic capsule length at the earliest sampled stage to ~145% in the adult cranium. This implies that the observed holocephalan pattern is not simply a case of enlarging the orbits relative to the skull, but also a simultaneous, pronounced negative allometry of the otic capsules.

**Data availability.** Materials used for the phylogenetic analysis in the current study are available in the Morphobank repository (<http://morphobank.org/>). Rendered CT data (STL files) of fossil and Recent specimens analysed in the current study are available in the Phenome10k repository (<http://phenome10k.org/>). The nodule-enclosed braincase of *D. oosthuizeni* Oelofsen<sup>8</sup> SAM K5840 is available for study in the collections of the South African Museum.

31. Swofford, D. L. *PAUP\*: Phylogenetic Analysis Using Parsimony (\*And Other Methods) v.4.0a147* (Sinauer Associates, 2003).
32. Felsenstein, J. Confidence-limits on phylogenies—an approach using the bootstrap. *Evolution* **39**, 783–791 (1985).
33. Bremer, K. The limits of amino-acid sequence data in angiosperm phylogenetic reconstruction. *Evolution* **42**, 795–803 (1988).
34. Eriksson, T. *AutoDecay Version 5.0*. (2001).
35. Rannala, B. & Yang, Z. Probability distribution of molecular evolutionary trees: a new method of phylogenetic inference. *J. Mol. Evol.* **43**, 304–311 (1996).
36. Yang, Z. & Rannala, B. Bayesian phylogenetic inference using DNA sequences: a Markov Chain Monte Carlo Method. *Mol. Biol. Evol.* **14**, 717–724 (1997).
37. Lewis, P. O. A likelihood approach to estimating phylogeny from discrete morphological character data. *Syst. Biol.* **50**, 913–925 (2001).
38. Ronquist, F. & Huelsenbeck, J. P. MrBayes 3: Bayesian phylogenetic inference under mixed models. *Bioinformatics* **19**, 1572–1574 (2003).
39. Ronquist, F. *et al.* MrBayes 3.2: efficient Bayesian phylogenetic inference and model choice across a large model space. *Syst. Biol.* **61**, 539–542 (2012).
40. Gradstein, F. M., Ogg, J. G., Schmitz, M. & Ogg, G. *The Geologic Time Scale 2012* (Elsevier, 2012).
41. Brazeau, M. D. & Friedman, M. The origin and early phylogenetic history of jawed vertebrates. *Nature* **520**, 490–497 (2015).
42. Young, G. C. Devonian sharks from south-eastern Australia and Antarctica. *Palaeontology* **25**, 817–843 (1982).
43. Gaudin, T. J. A re-examination of elasmobranch monophyly and chondrichthyan phylogeny. *Jb. Geol. Palaont. Abh.* **182**, 133–160 (1991).
44. Lund, R. & Grogan, E. D. Relationships of the Chimaeriformes and the basal radiation of the Chondrichthyes. *Rev. Fish Biol. Fish.* **7**, 65–123 (1997).
45. Ginter, M., Hampe, O. & Duffin, C. in *Handbook of Paleoichthyology* Vol. 3D (ed. Schultze, H.-P.) (Friedrich Pfeil, 2010).
46. Davis, S. P., Finarelli, J. A. & Coates, M. I. *Acanthodes* and shark-like conditions in the last common ancestor of modern gnathostomes. *Nature* **486**, 247–250 (2012).
47. Zhu, M. *et al.* A Silurian placoderm with osteichthyan-like marginal jaw bones. *Nature* **502**, 188–193 (2013).
48. Dupret, V., Sanchez, S., Goujet, D., Tafforeau, P. & Ahlberg, P. E. A. A primitive placoderm sheds light on the origin of the jawed vertebrate face. *Nature* **507**, 500–503 (2014).
49. Janvier, P. & Pradel, A. in *Physiology of Elasmobranch Fishes: Structure and Interaction with Environment* (eds Shadwick, R. E., Farrell, A. P. & Brauner, C. J.) (Academic, 2016).
50. Maisey, J. G. Chondrichthyan phylogeny: a look at the evidence. *J. Vertebr. Paleontol.* **4**, 359–371 (1984).
51. Zangerl, R. in *Handbook of Paleoichthyology* Vol. 3A (ed. Schultze, H.-P.) (Gustav Fischer, 1981).
52. Zangerl, R. in *Mazon Creek Fossils* (ed. Nitecki, M. H.) 449–500 (Academic, 1979).
53. Tapanila, L. *et al.* Jaws for a spiral-tooth whorl: CT images reveal novel adaptation and phylogeny in fossil *Helicoprion*. *Biol. Lett.* **9**, 20130057 (2013).
54. Benton, M. J. *et al.* Constraints on the timescale of animal evolutionary history. *Palaeontologia Electronica* **18**, 1–116 (2015).
55. Darras, L., Derycke, C., Blicke, A. & Vachard, D. The oldest holocephalan (Chondrichthyes) from the Middle Devonian of the Boulonnais (Pas-de-Calais, France). *C. R. Palevol* **7**, 297–304 (2008).
56. Gardiner, B. G. The relationships of the palaeoniscid fishes, a review based on new specimens of *Mimia* and *Moythomasia* from the Upper Devonian of Western Australia. *Bull. Br. Mus. Nat. Hist.* **37**, 173–428 (1984).

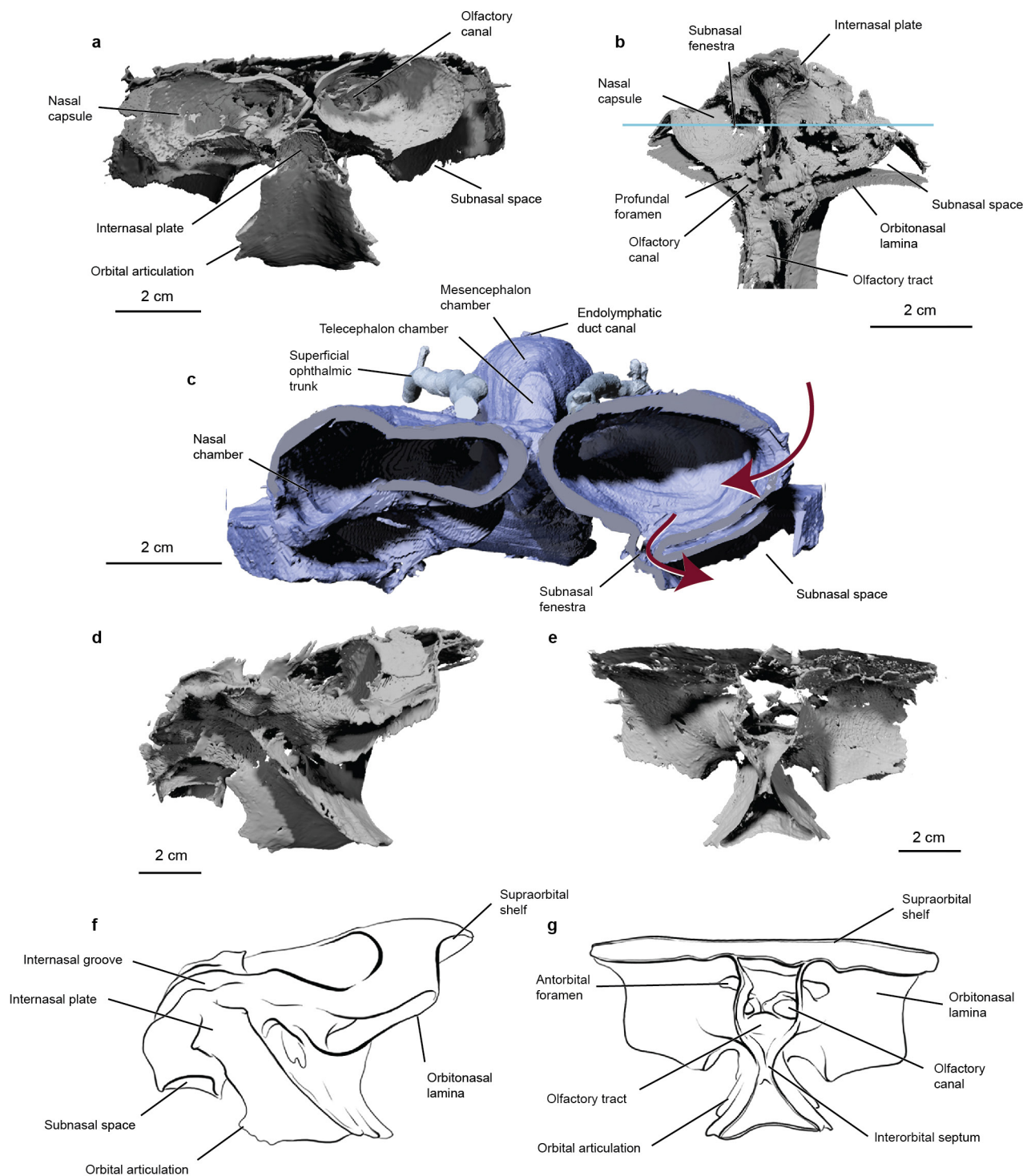


**Extended Data Figure 1** | *D. oosthuizeni* Oelofsen 1986 SAM K584, the nodule. **a**, Ventral part, showing infilled orbits, ethmoid region floor and floor of otic and occipital regions in dorsal view; anterior to left. **b**, Nodule in lateral view, showing division between dorsal and ventral sections. **c**, Dorsal part, showing infilled nasal capsules, supraorbital shelves, and endocranium in ventral view. Anterior to right in **b** and **c**. **d**, Area of tessellate calcified cartilage.



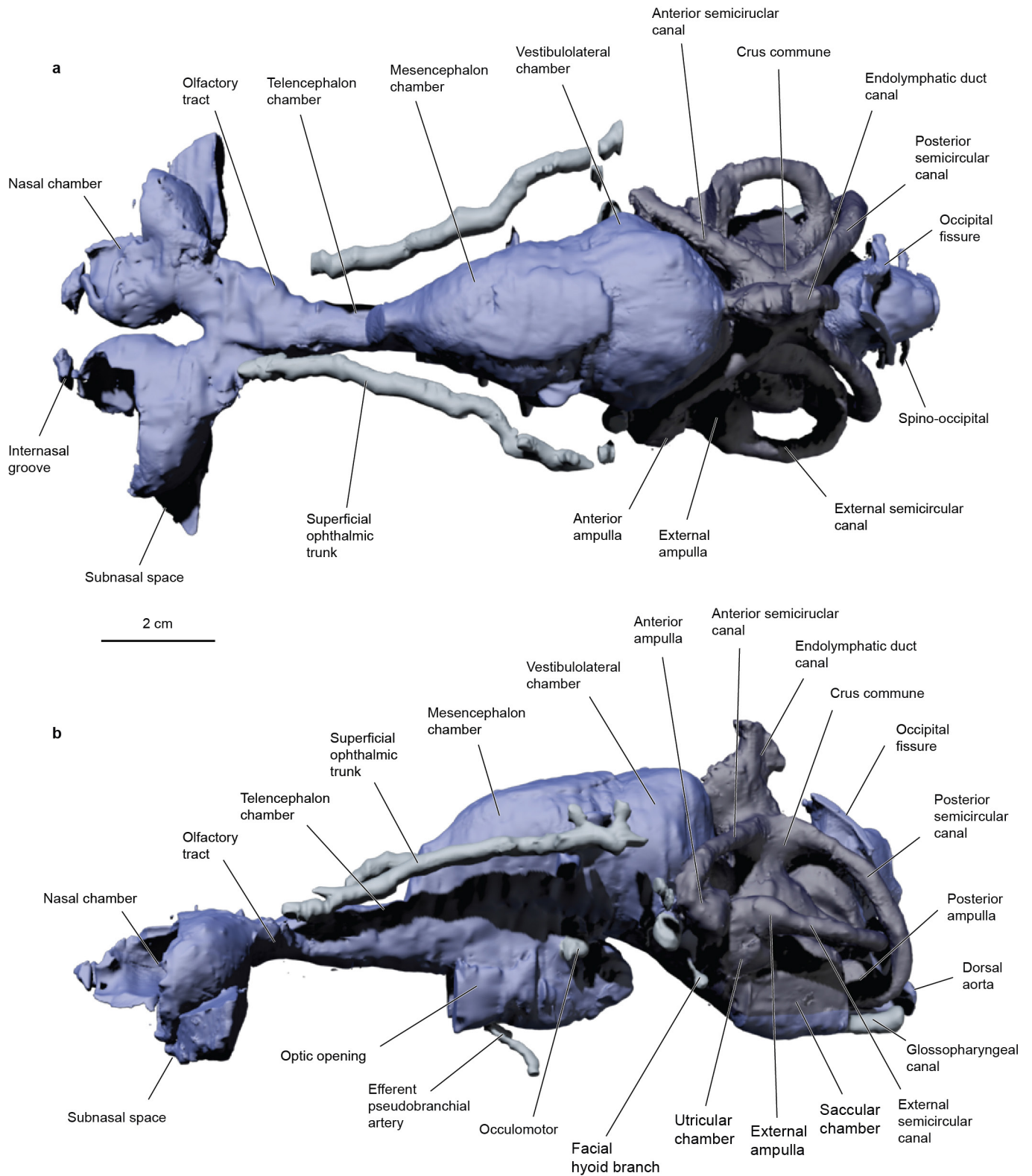
**Extended Data Figure 2 | Comparison of symmoriiform braincases.**  
**a**, FMNH PF 13242, lateral view, drawn from figure 6 in ref. 9. **b**, FMNH 13242, ventral view, drawn from figure 8 in ref. 9. **c**, *Cobelodus*, FMNH PF 7345, drawn from figure 5b in ref. 11. **d**, *Ozarcus*, AMNH FF 20544, lateral view, drawn from extended data figure 2h in ref. 13, grey area

signifies material missing in **a**. **e**, *Ozarcus*, AMNH FF 20544, ventral view, adapted from extended data figure 2h in ref. 13, Nature Publishing Group. **f**, *Dwykaselachus*, lateral view restored. **g**, *Dwykaselachus*, ventral view restored. **h**, *Akmonistion*, NMS 1981.63.22C, ventral view, drawn from figure 1c in ref. 10.

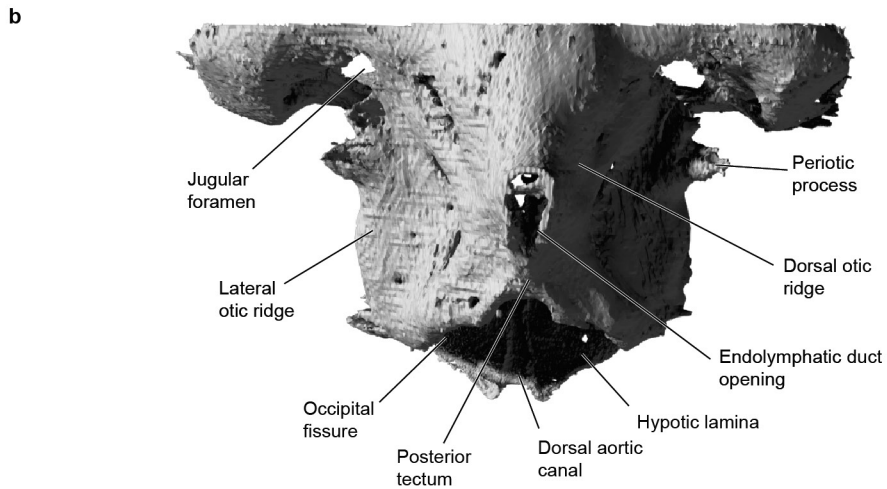
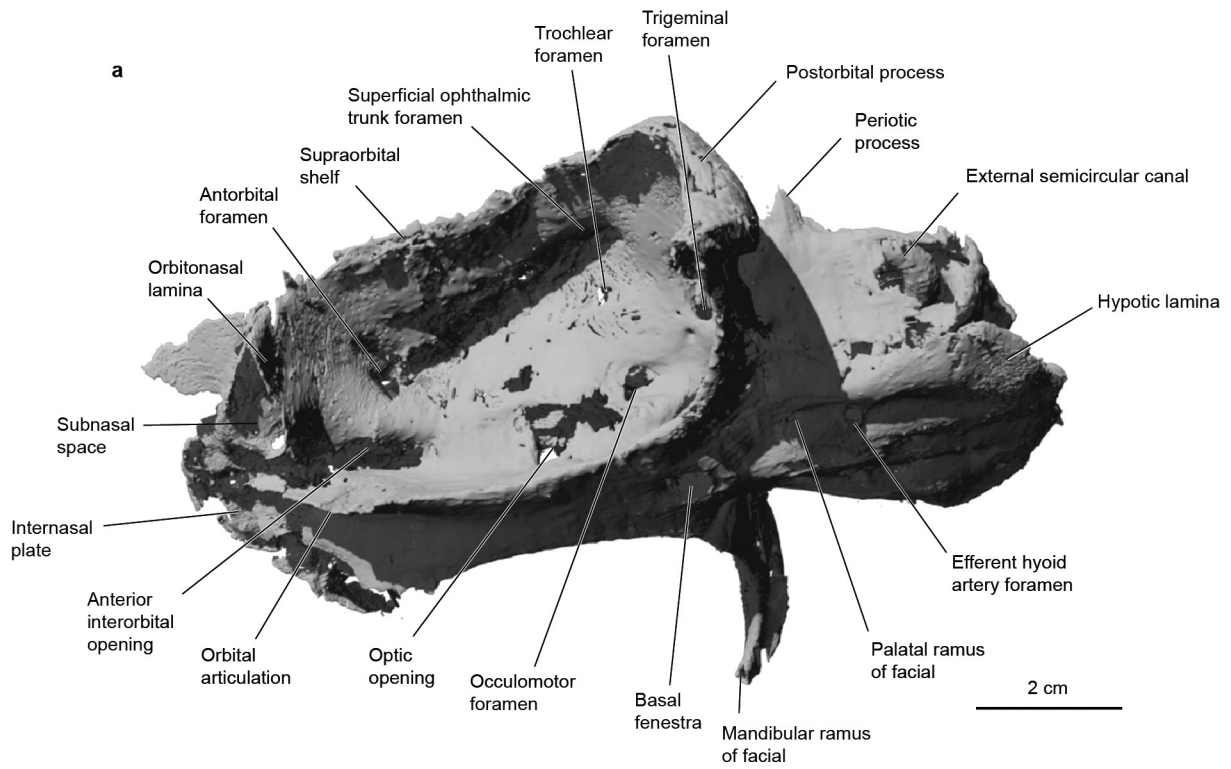


**Extended Data Figure 3 | Ethmoid region of *Dwykaselachus* based on CT rendering of SAM K584. a**, Anterior view with material anterior to blue line in **b** removed. **b**, Dorsal view of nasal capsules and anterior portion of interorbital space, modelled as if sectioned horizontally at mid-capsular level; horizontal blue line indicates level of sections shown in **a** and **c**. **c**, Anterior view of endocranial spaces incompletely infilled to show pattern of interconnecting chambers (model sectioned vertically at mid-nasal capsule level, as indicated by blue line in **b**). The subnasal space

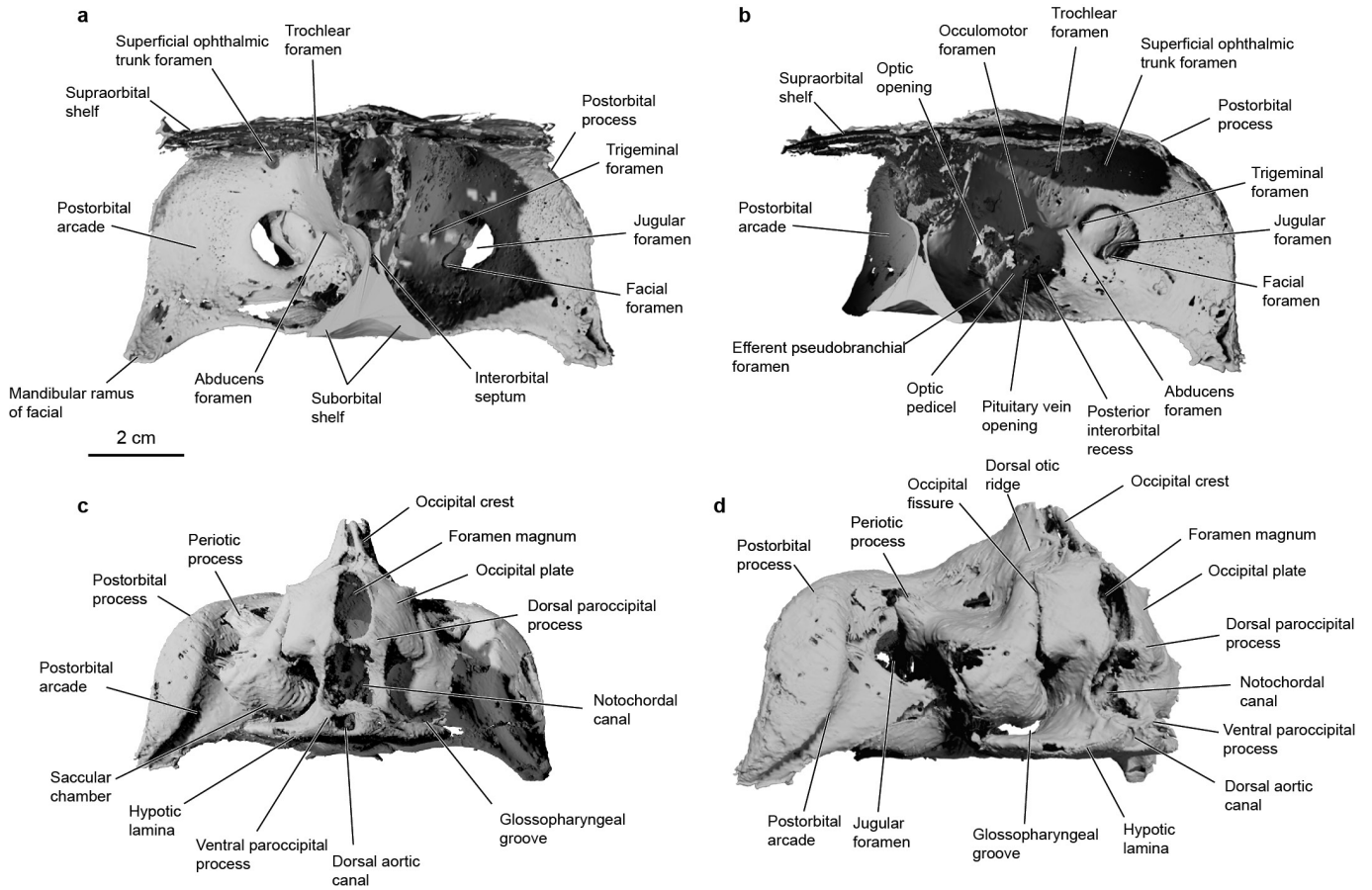
may have formed a cartilage-filled antorbital process (see also Extended Data Fig. 5a), but the communication with the nasal capsule via the subnasal fenestra raises the possibility that it housed an accessory nasal duct, resembling those in modern chimaeroids<sup>1,22</sup>; arrows suggest possible direction of water flow. **d**, Anterolateral and ventral aspect. **e**, Posterior view of ethmoid region, model sectioned across anterior of orbit. **f**, **g**, Line drawings of **d** and **e**, respectively.



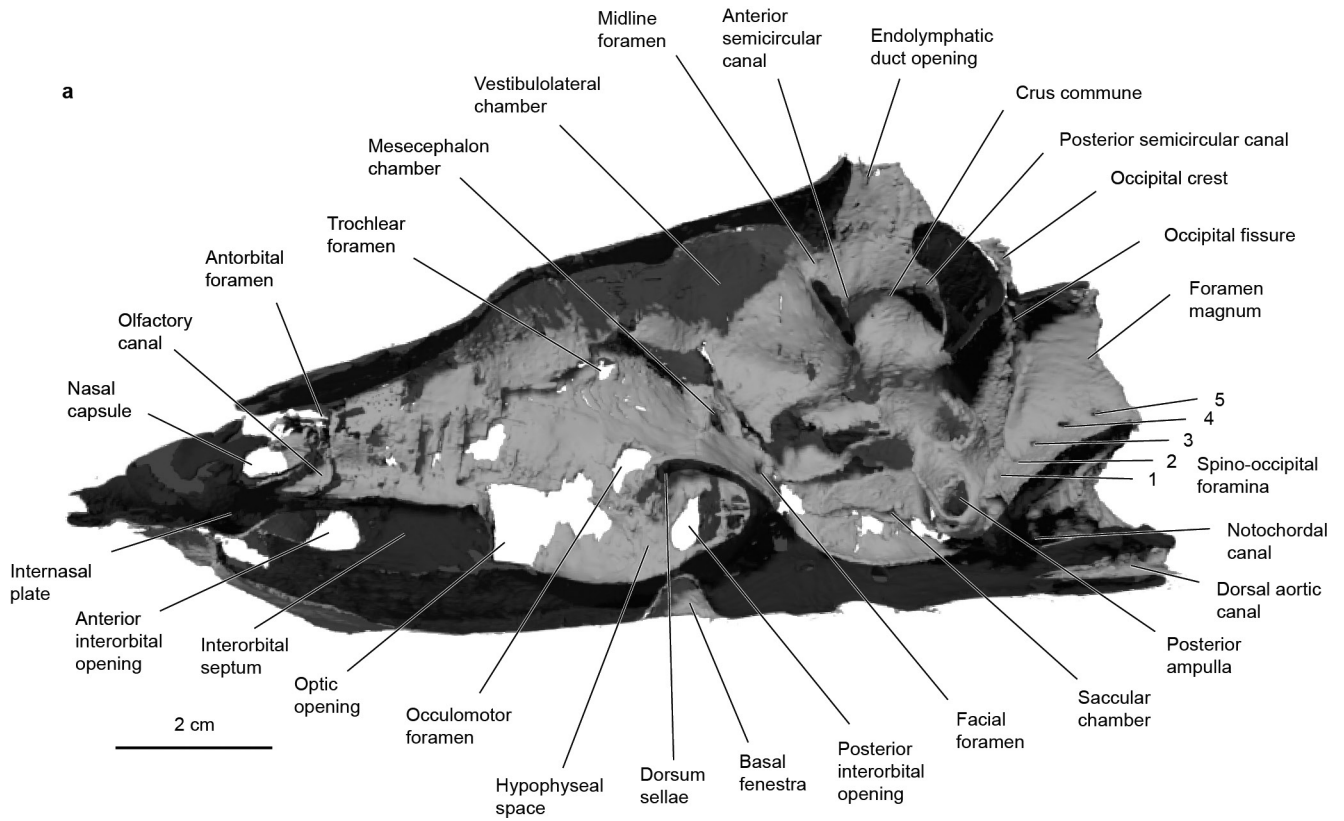
**Extended Data Figure 4 | Endocast morphology of *D. oosthuizeni* SAM K5840. a, b, CT rendering of cranial endocast, semicircular canals and ampullae, and path of superficial ophthalmic nerves in dorsal view (a) and in lateral view (b).**



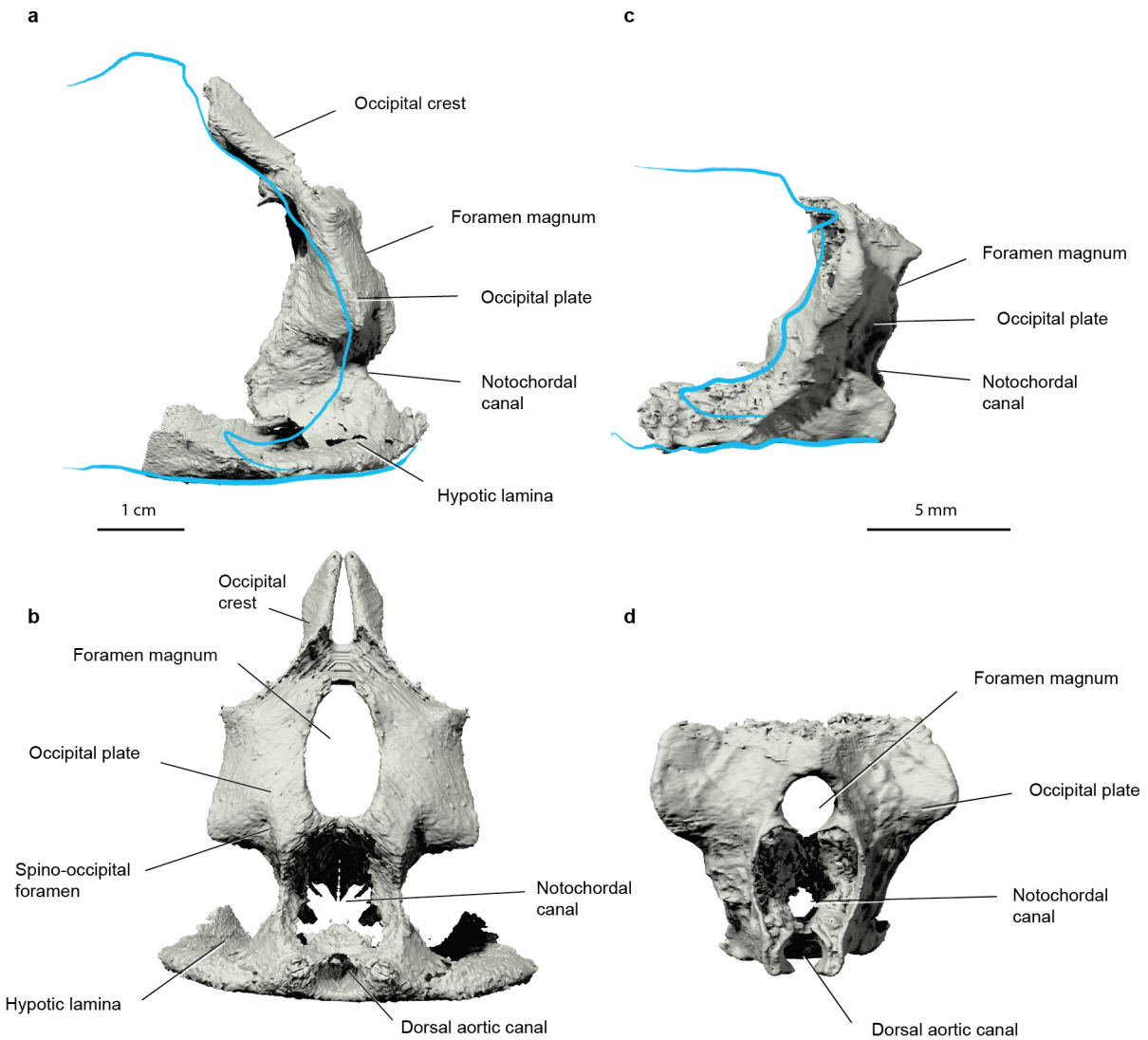
**Extended Data Figure 5 | *D. oosthuizeni* SAM K5840 braincase. a, CT rendering in ventrolateral view. b, Rendering of braincase roof, posterior to level of postorbital process, with occipital arch removed to show posterior tectum.**



**Extended Data Figure 6 | *D. oosthuizeni* SAM K5840 braincase.** **a**, Anterior view of CT rendering of postorbital wall, as if the braincase is cross-sectioned (clipped) at mid-orbit level. **b**, Anterolateral view of same. Removal of ethmoid region permits an unobstructed view. **c**, **d**, CT rendering of braincase in posterior view (**c**) and posterolateral view (**d**).

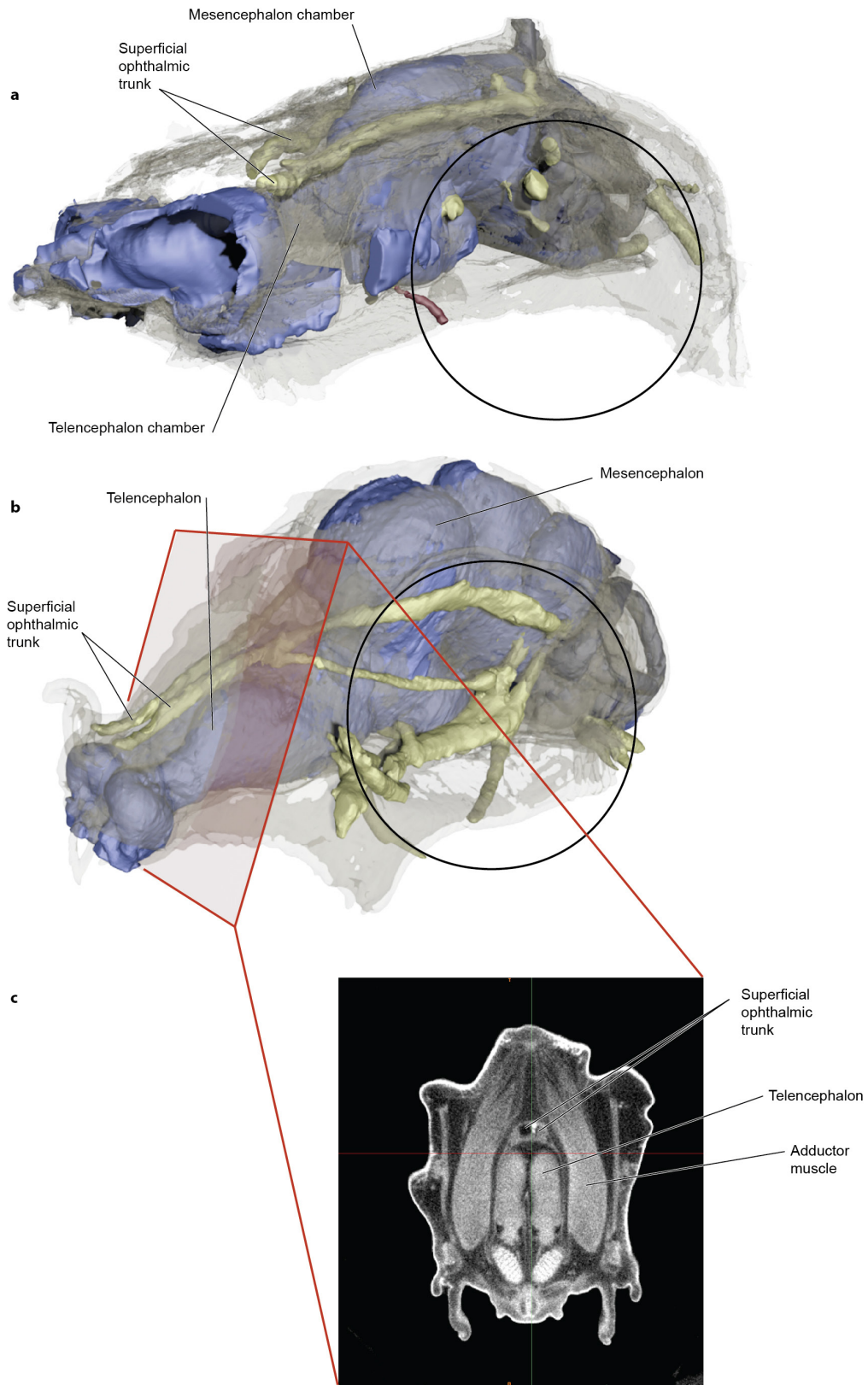


**Extended Data Figure 7** | *D. oosthuizeni* SAM K5840 braincase. Medial view of sagittal section of CT rendered neurocranium, showing endocranial spaces.

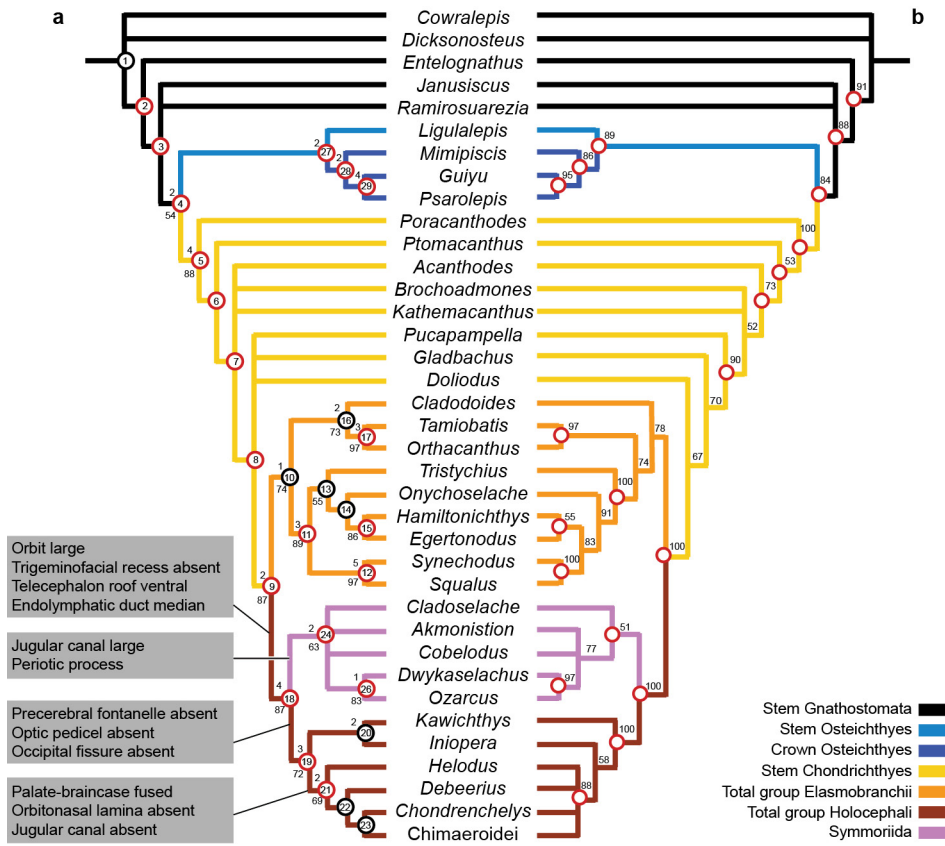


**Extended Data Figure 8 | Symmoriiform and osteichthyan (actinopterygian) occipital arches.** **a, b**, *Dwykasselachus* in lateral and posterior views; model based on mirrored right side CT of SAM K5840. **c, d**, *Moythomasia durgaringa* Gardiner & Bartram in lateral and posterior views, model based on CT of MV P222915 (dorsal portion of occipital

plate missing). Blue line in **a** and **c** indicates profile of braincase posterior extremity of the otic capsule; profile for *Moythomasia*, drawn from ref. 56. In both examples, the dorsal part of the occipital arch does not project anteriorly between the otic capsules (unlike elasmobranch conditions).



**Extended Data Figure 9** | *Dwykaselachus* and *Callorhynchus* crania rendered semi-transparent in anterolateral view. **a**, **b**, *Dwykaselachus*, model based on CT of SAM K5840 (**a**) and *Callorhynchus*, revealing relation of superficial ophthalmic trunks to forebrain, and forebrain level relative to dorsally prominent mesencephalon (**b**). **c**, *Callorhynchus* CT coronal preorbital slice linked to framed section in **b**; ellipses (black line) indicate orbit size.



**Extended Data Figure 10 | Consensus trees from phylogenetic analyses.** **a**, Maximum parsimony analysis. Strict consensus of 240 most parsimonious trees; node numbers ringed (character state transitions listed in Supplementary Table 2); numbers above branches are Bremer support scores and numbers below are bootstrap values. Character state summaries (grey boxes) list neurocranial changes at basal nodes within

the total group Holocephali. **b**, Bayesian analysis. Majority rule consensus tree; numbers above branches are the posterior probabilities, measured as proportion of sampled trees in which that topology was recovered. Nodes ringed in red are recovered in both the maximum parsimony and Bayesian analyses.